arXiv:1408.2256v2 [cond-mat.quant-gas] 17 Sep 2014

Localized modes in quasi-2D Bose-Einstein condensates with spin-orbit and Rabi couplings

Luca Salasnich,[1,2] Wesley B. Cardoso,[3] and Boris A. Malomed[4]

[1]*Dipartimento di Fisica e Astronomia "Galileo Galilei" and CNISM, Università di Padova, Via Marzolo 8, 35131 Padova, Italy*
[2]*Istituto Nazionale di Ottica (INO) del Consiglio Nazionale delle Ricerche (CNR), Sezione di Sesto Fiorentino, Via Nello Carrara, 1 - 50019 Sesto Fiorentino, Italy*
[3]*Instituto de Física, Universidade Federal de Goiás, 74.001-970, Goiânia, Goiás, Brazil*
[4]*Department of Interdisciplinary Studies, School of Electrical Engineering, Faculty of Engineering, Tel Aviv University, Tel Aviv 69978, Israel*

We consider a two-component pancake-shaped, i.e., effectively two-dimensional (2D), Bose-Einstein condensate (BEC) coupled by the spin-orbit (SO) and Rabi terms. The SO coupling adopted here is of the mixed Rashba-Dresselhaus type. For this configuration, we derive a system of two 2D nonpolynomial Schrödinger equations (NPSEs), for both attractive and repulsive interatomic interactions. In the low- and high-density limits, the system amounts to previously known models, namely, the usual 2D Gross-Pitaevskii equation, or the Schrödinger equation with the nonlinearity of power $7/3$. We present simple approximate localized solutions, obtained by treating the SO and Rabi terms as perturbations. Localized solutions of the full NPSE system are obtained in a numerical form. Remarkably, in the case of the attractive nonlinearity acting in free space (i.e., without any 2D trapping potential), we find parameter regions where the SO and Rabi couplings make 2D fundamental solitons dynamically stable.

PACS numbers: 03.75.Ss, 03.75.Hh, 64.75.+g

I. INTRODUCTION

The Bose-Einstein condensates (BECs) have become an important ground for the study of macroscopic quantum phenomena. The first experimental realizations in 1995 were implemented using rubidium [1], sodium [2], and lithium [3] atoms, which motivated a great deal of work [4] on topics such as the Anderson localization of matter waves [5, 6], production of bright [7–10] and dark solitons [11], dark-bright complexes [12], vortices [13] and vortex-antivortex dipoles [14–17], persistent flows in the toroidal geometry [18, 19], skyrmions [20], emulation of gauge fields [21] and spin-orbit (SO) coupling [22], quantum Newton's cradles [23], *etc*.

The recent realization of the artificial SO coupling in a neutral atomic BEC [22] was an incentive for many more works, dealing, in particular, with vortex structures in rotating SO-coupled BECs [24–27] and trapped 2D atomic BEC with spin-independent interactions in the presence of the isotropic SO coupling [28, 29], which shows that, for weak interactions, two types of half-vortex solutions with different winding numbers occur. Further, in the weakly interacting regime realized for the two-component Bose gas in a 2D harmonic-oscillator (HO) trap, subject to isotropic SO coupling of the Rashba type, it was found that the condensate's ground state has a half-quantum angular momentum vortex configuration with spatial rotational symmetry and skyrmion-type spin texture [30]. The introduction of order by disorder in Rashba-SO-coupled BECs was demonstrated in Ref. [31]. In Ref. [32], an experimental scheme was proposed for the creation of the SO coupling in spin-3 Cr atoms, using the Raman illumination, and the ground-state properties of that model were studied. In Ref. [33], the ground-state properties of a weakly trapped spin-1 BEC with the SO coupling were studied by means of numerical and analytical methods in an external Zeeman field. The existence of complex, antiferromagnetically ordered (striped), ground states in the 1D SO-coupled system with the repulsive interactions and external HO trap was demonstrated in Ref. [34].

Bright solitons in the BEC with the SO coupling were introduced in Refs. [35–38] and [39, 40], in the 1D and 2D geometries, respectively. In particular, in Ref. [38] localized modes in dense repulsive and attractive BECs with the spin-orbit and Rabi couplings were investigated; Ref. [37] reported a diversity of stable gap solitons in the SO-coupled BEC subject to the action of a spatially periodic Zeeman field; employing a multiscale-expansion method, bright-solitons families and three different dark soliton families were found, respectively in Refs. [36] and [41] (the dark solitons could be supported by either a constant or a spatially modulated background density). As concerns 2D bright solitons, an unexpected results was reported in Ref. [39]: two different families of vortex solitons, namely semi-vortices (with topological charges $m = 0$ and ± 1 in the two components) and mixed modes (which combine $m = 0$ and ± 1 in each component) are *stable* in the 2D binary BEC with the Rashba coupling in the *free space*, without the support of any trapping potential, while it commonly believed that all 2D free-space solitons are unstable in the presence of the cubic attractive nonlinearity due to the occurrence of the critical collapse in the same setting [42]. Various families of 2D localized solutions, including multipole and half-vortex solitons featuring various symmetries with respect to the parity and time reversal in a lattice created by the Zeeman field were reported in Ref. [40] for the mixed Rashba-Dresselhaus SO coupling.

The stability of plane waves in the the two-dimensional SO-coupled BEC was studied analytically in Refs. [43, 44]. Vortex-lattice solutions to the coupled Gross-Pitaevskii (GP) equations with the SO coupling and optical-lattice potential were reported in Ref. [45]. Vortex dynamics in the SO-coupled BEC was studied in Ref. [46], while Ref. [47]

addresses the existence of the vortex-antivortex-pair lattices in the BEC with the Rashba SO coupling. Recently, Ref. [48] reported, by means if numerical and variational methods, the localization of a noninteracting and weakly interacting SO-coupled BEC in a quasiperiodic bichromatic optical-lattice potential, confirming the existence of stationary localized states in the presence of the SO and Rabi couplings for equal numbers of atoms in the two components. In Ref. [49], transitions of ground states, induced by the zero-momentum coupling in the Rashba-SO-coupled BEC with pseudospin 1/2 were investigated in the presence of the confining HO potential. Fragmentation of SO-coupled spinor BEC was studied in Ref. [50], and Anderson localization of cold atomic gases with the effective spin-orbit interaction in a quasiperiodic optical lattice was theoretically investigated in Ref. [51].

Most works dealing with patterns produced by the SO coupling used GP equations with the cubic nonlinearity. However, it is known that a sufficiently strong transverse confinement leads to effective nonlinearity which is different from cubic, thus given rise to nonpolynomial Schrödinger equations (NPSEs) [52, 53]. In particular, in Ref. [38] a system of coupled 1D NPSEs was derived from the full 3D two-component GP equations including the SO and Rabi couplings. In the case of the attractive nonlinearity, this effective 1D system features essential reduction of the collapse threshold, under the action of the SO and Rabi couplings, suggesting an expansion of the range of physical parameters where experiments may reveal new self-trapped modes. The variety of the above-mentioned theoretical results obtained for the SO-coupled BEC in the effectively 2D geometry suggests the relevance of deriving an effective 2D NPSE system, starting from the full set of 3D GP equations with the SO and Rabi couplings, and taking into regard the strong confinement in the direction perpendicular to the 2D "pancake". The derivation of such a system, and analysis of localized solutions (solitons) predicted by it, is the subject of the present work.

The paper is organized as follows. The derivation of the 2D NPSEs system is presented in Sec. II. along with simple analytical approximations for localized modes produced by these equations, and the low- and high-density limit cases. Numerical results for the localized states, obtained in the system with the self-attractive and self-repulsive interactions are reported in Sec. III. The paper is concluded by Sec. IV.

II. NONPOLYNOMIAL SCHRÖDINGER EQUATIONS FOR THE SPIN-ORBIT-COUPLED CONDENSATE

The single-particle Hamiltonian with the SO-coupling term (of the mixed Rashba-Dresselhaus type), which can be implemented in BEC, is

$$\hat{h}_{\rm SP} = \left[\frac{\hat{\mathbf{p}}^2}{2m} + U(\mathbf{r})\right] + \frac{\hbar\Omega}{2}\sigma_x - \frac{k_L}{m}\hat{p}_x\sigma_z, \qquad (1)$$

where $\hat{\mathbf{p}} = -i\hbar(\partial_x, \partial_y, \partial_z)$ is the momentum operator, $U(\mathbf{r})$ is a trapping potential, k_L is the recoil wavenumber induced by the interaction with the laser beams, Ω is the frequency of the Raman coupling, which is responsible for the linear mixing between the two states, and $\sigma_{x,y,z}$ are the Pauli matrices.

A. Derivation of the model

The dilute SO- and Rabi-coupled binary BEC, confined in the z direction by a tight HO potential with trapping frequency ω_z, and in the (x, y) plane by a generic loose potential $V(x, y)$, is governed by the system of 3D GPEs for macroscopic wave functions $\Psi_k(x, y, z, t)$ of the two atomic states ($k = 1, 2$):

$$i\partial_t\Psi_k = \left[-\frac{1}{2}\nabla^2 + V(x,y) + \frac{1}{2}z^2 + (-1)^{k-1}i\gamma\partial_x + \sqrt{2\pi}g_k|\Psi_k|^2 + \sqrt{2\pi}g_{12}|\Psi_{3-k}|^2\right]\Psi_k + \Gamma\Psi_{3-k}, \qquad (2)$$

where the lengths, time, and energy are measured in units of $a_z = \sqrt{\hbar/(m\omega_z)}$, ω_z^{-1}, and $\hbar\omega_z$, respectively. Here $g_k \equiv \sqrt{2\pi}(2a_k/a_z)$, $g_{12} \equiv \sqrt{2\pi}(2a_{12}/a_z)$ are strengths of the intra- and inter-species interactions, where a_k and a_{12} are the respective scattering lengths, while $\gamma = k_L a_z$ and $\Gamma = \Omega/(2\omega_z)$ are dimensionless strengths of the spin-orbit and Rabi couplings, respectively. The time-dependent number of atoms in the k-th state is $N_k(t) = \int\int\int dxdydz|\Psi_k(x, y, z, t)|^2$, the constant total number of atoms being $N = N_1(t) + N_2(t)$.

In most cases, a reasonable assumption is that strengths of the nonlinear interactions between different atomic states are equal, $g_1 = g_2 = g_{12} \equiv g$ [54]. Under this condition, we aim to construct stationary states with chemical potential μ, by setting

$$\Psi_k(x, y, z, t) = \psi_k(x, y, z)\, e^{-i\mu t} \qquad (3)$$

in Eq. (2). The resulting equations for stationary fields $\psi_{1,2}(x, y, z)$ are compatible with the restriction

$$\psi_1^*(x, y, z) = \psi_2(x, y, z), \qquad (4)$$

which leads to the single stationary equation:

$$\mu\Phi = \left[-\frac{1}{2}\nabla^2 + V(x,y) + \frac{1}{2}z^2 + i\gamma\partial_x + \sqrt{2\pi}g|\Phi|^2\right]\Phi + \Gamma\Phi^*, \qquad (5)$$

where we set $\Phi(x, y, z) \equiv \sqrt{2/N}\psi_1(x, y, z) = \sqrt{2/N}\psi_2^*(x, y, z)$, so that $\int\int\int dxdydz|\Phi(x, y, z)|^2 = 1$.

To simplify the stationary 3D problem, we adopt the usual factorized ansatz for the wave functions which are strongly confined in the direction of z, and weakly confined in the plane of (x, y):

$$\Psi_k(x, y, z, t) = \frac{\exp\left[-(1/2)\eta_k^2(x, y, t)z^2\right]}{\pi^{1/4}\sqrt{\eta_k(x, y, t)}}F_k(x, y, t), \qquad (6)$$

where $\eta_k(x,y,t)$ and $F_k(x,y,t)$ are the axial width and planar wave function, respectively, the latter normalized by conditions

$$\int\int dxdy|F_k(x,y)|^2 = 1. \tag{7}$$

Inserting ansatz (6) into the energy functional which produces Eq. (5), performing the integration in the transverse plane, and neglecting, as usual, derivatives of $\eta_k(x,y)$, we derive the corresponding effective energy functional, which reduces 3D equations (2) to a system of two effectively 2D equations:

$$\begin{aligned} i(F_k)_t &= \left[-\frac{1}{2}(\partial_x^2+\partial_y^2) + V(x,y) + (-1)^{k-1}i\gamma\partial_x \right. \\ &+ \left. \frac{1}{4}\left(\frac{1}{\eta_k^2}+\eta_k^2\right) + \frac{g}{\eta_k}|F_k|^2\right]F_k + \Gamma F_{3-k}, \end{aligned} \tag{8}$$

$$\eta_k^4 = 1 + g|F_k|^2\eta_k. \tag{9}$$

Further, stationary 2D solutions may be looked for as

$$F_k(x,y,t) = e^{-i\mu t}f_k(x,y) \tag{10}$$

$$f_1(x,y) = f_2^*(x,y) \equiv f(x,y),\ \eta_1(x,y) = \eta_2(x,y) \equiv \eta(x,y) \tag{11}$$

[cf. Eqs. (3), (4)], with complex function $f(x,y)$ and real one $\eta(x,y)$ obeying the following equations:

$$\begin{aligned} \mu f &= \left[-\frac{1}{2}(\partial_x^2+\partial_y^2) + V(x,y) + i\gamma\partial_x \right. \\ &+ \left. \frac{1}{4}\left(\frac{1}{\eta^2}+\eta^2\right) + \frac{g}{\eta}|f|^2\right]f + \Gamma f, \end{aligned} \tag{12}$$

$$\eta^4 = 1 + g|f|^2\eta. \tag{13}$$

The energy (Hamiltonian) of the 2D system is (in the most general case, without assuming relation $f_1 = f_2^*$ and $\eta_1 = \eta_2$) $H = \int\int dxdy\mathcal{H}$, with density

$$\begin{aligned} \mathcal{H} = \sum_{k=1}^{2}\left\{\frac{1}{2}|\nabla f_k|^2 + V(x,y)|f_k|^2 \right. \\ +(-1)^{k-1}\frac{i}{2}\gamma\left[f_k^*\left(f_k\right)_x - f_k\left(f_k^*\right)_x\right] \\ \left. + \frac{1}{4}\left(\frac{1}{\eta_k^2}+\eta_k^2\right)|f_k|^2 + \frac{g}{2\eta_k}|f_k|^4 + \Gamma f_k f_{3-k}^*\right\}. \end{aligned} \tag{14}$$

In the case when restrictions $f_1 = f_2^*$ and $\eta_1 = \eta_2$ are imposed, Hamiltonian (14) simplifies to

$$\begin{aligned} \mathcal{H} &= |\nabla f|^2 + 2V(x,y)|f|^2 + i\gamma\left[f^*\left(f\right)_x - f\left(f^*\right)_x\right] \\ &+ \frac{1}{2}\left(\frac{1}{\eta^2}+\eta^2\right)|f|^2 + \frac{g}{\eta}|f|^4 + \Gamma\left[f^2 + (f^*)^2\right]. \end{aligned} \tag{15}$$

Exact solutions to Eq. (13) may be given by the Cardano formula,

$$\begin{aligned} \eta = \pm\frac{1}{2}\sqrt{\frac{A^2-12}{3A}} \\ +\frac{1}{2}\sqrt{-\frac{A^2-12}{3A} \pm 2g|f|^2\left(\frac{A^2-12}{3A}\right)^{-1/2}}, \end{aligned} \tag{16}$$

where the upper and lower signs correspond, respectively, to $g > 0$ and $g < 0$, and

$$A \equiv (3/2)^{1/3}\left(9g^2|f|^4 + \sqrt{3}\sqrt{256+27g^4|f|^8}\right)^{1/3}. \tag{17}$$

Inserting Eq. (16) into Eq. (12) one gets a 2D NPSE, which is a generalization of that introduced earlier for the study of solitons and solitary vortices in "pancake"-shaped Bose-Einstein condensates [52, 55].

B. Simple analytical approximations

Following the consideration of the 1D counterpart of this system in Ref. [38], a simple analytical approximation can be obtained from Eq. (12) for large Γ:

$$f(x,y;\mu) \approx \left[1 + \frac{i\gamma}{\Gamma}\partial_x\right]f_0(x,y;\mu'),\ \mu' \equiv \mu - \Gamma, \tag{18}$$

where $f_0(x,y)$ is a real solution obtained from Eqs. (12) and (13) with $\Gamma = \gamma = 0$ and μ replaced by μ'. Thus, at large Γ the solution acquires a small imaginary part given by Eq. (18).

The term $\sim\gamma$ can be eliminated from Eq. (12) by means of substitution [38]

$$f(x,y;\mu) = e^{i\gamma x}\widetilde{f}(x,y;\widetilde{\mu}),\ \widetilde{\mu} \equiv \mu - \gamma^2/4, \tag{19}$$

which transforms Eqs. (12) and (13) into the following form:

$$\begin{aligned} \widetilde{\mu}\widetilde{f} &= \left[-\frac{1}{2}(\partial_x^2+\partial_y^2) + V(x,y) \right. \\ &+ \left. \frac{1}{4}\left(\frac{1}{\widetilde{\eta}^2}+\widetilde{\eta}^2\right) + \frac{g}{\widetilde{\eta}}|\widetilde{f}|^2\right]\widetilde{f} + \Gamma e^{-2i\gamma x}\widetilde{f}, \end{aligned} \tag{20}$$

$$\widetilde{\eta}^4 = 1 + g|\widetilde{f}|^2\widetilde{\eta}. \tag{21}$$

Thus, in the absence of the Rabi term ($\Gamma = 0$), the SO coupling drops from Eq. (20). Again following the lines of Ref. [38], an approximate solution to Eq. (20) can be constructed for the limit of large γ:

$$\widetilde{f}(x,y;\mu) \approx \left[1 - \frac{\Gamma}{\gamma^2}e^{-2i\gamma x}\right]\widetilde{f}_0(x,y;\widetilde{\mu}), \tag{22}$$

where $\widetilde{f}_0(x,y;\widetilde{\mu})$ stands for the usual real solution to Eqs. (20) and (21) with $\widetilde{\mu}$ taken as per Eq. (19).

C. Low- and high-density limits

In the low-density limit, $|g||f|^2 \ll 1$, Eq. (13) yields a simple solution,

$$\eta_{\rm low} \simeq 1 + g|f|^2/4. \tag{23}$$

The substitution of this approximation in Eq. (12) reduces it to the NPSE with the cubic-quintic nonlinearity, in which the quintic term always corresponds to the effective self-attraction:

$$\left(\mu - \frac{1}{2}\right) f = \left[-\frac{1}{2}(\partial_x^2 + \partial_y^2) + V(x,y) + i\gamma\partial_x + g|f|^2 - \frac{3}{16}g^2|f|^4\right] f + \Gamma f^*. \tag{24}$$

In the high-density limit, $|g||f|^2 \gg 1$, asymptotic expressions for the axial width which follow from Eq. (13) are different in the cases of repulsion ($g > 0$) and attraction ($g < 0$),

$$\eta_{\rm high}^{\rm (rep)} \simeq (g|f|^2)^{1/3}, \quad \eta_{\rm high}^{\rm (attr)} \simeq -(g|f|^2)^{-1}. \tag{25}$$

The substitution of these approximations in Eq. (12) leads to two different 2D NPSEs: in the case of repulsion, it is

$$\mu f = \left[-\frac{1}{2}(\partial_x^2 + \partial_y^2) + V(x,y) + i\gamma\partial_x + \frac{5}{4}g^{2/3}|f|^{4/3}\right] f + \Gamma f^*, \tag{26}$$

and in the case of attraction, the effective equation is the NPSE with the quintic term only:

$$\mu f = \left[-\frac{1}{2}(\partial_x^2 + \partial_y^2) + V(x,y) + i\gamma\partial_x - \frac{3}{4}g^2|f|^4\right] f + \Gamma f. \tag{27}$$

Figure 1 shows the behavior of the axial width η as a function of $g|f|^2$ for the different cases presented above. The exact solution for η (given by Eq. (16)) is displayed by the solid (black) line. The solution for the low-density limit [Eqs. (23)] is presented by the dashed (green) line, while circles (yellow) and boxes (red) represents the high-density repulsive and attractive limits, respectively, see Eq. (25).

III. NUMERICAL RESULTS

We start by present the numerical results for the effective 2D stationary equation (12). To this end, we have employed a split-step algorithm that uses the imaginary-time propagation (ITP) to generate the ground-state solution of the system. The ITP method includes the restoration the original norm (7) of the solution at the end of each step of marching forward in imaginary time. To this end, Eq. (12) was replaced by

$$iF_t = (H_d + H_{nd})F + \Gamma F^*, \tag{28}$$

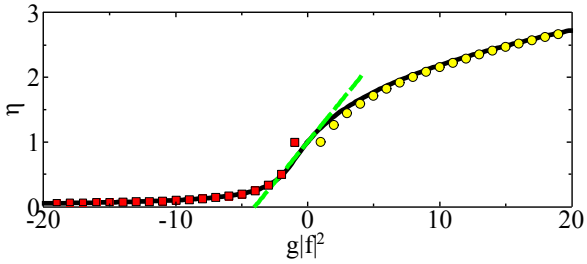

Figure 1: (Color online) The axial width η of the pancake-shaped condensate versus $g|f|^2$. The solid (black) curve displays the behavior of η given by the Eq. (16); by the dashed (green) line we show the low-density limit [Eq. (23)]; the high-density limit for the repulsive and attractive cases [Eq. (25)] are shown by circles (yellow) and boxes (red), respectively.

where

$$H_d \equiv -\frac{1}{2}\left(\partial_x^2 + \partial_y^2\right) + i\gamma\partial_x, \tag{29}$$

$$H_{nd} \equiv V(x,y) + G(|F|^2), \tag{30}$$

and $F \equiv F_1 = F_2^*$ [cf. Eqs. (10) and (11)], the subscripts d and nd referring to the derivative and non-derivative terms, respectively, and $G(|F|^2)$ is the nonlinear term of the equation that we aim to solve. For the implementation of the ITP method, we change $t \to -it$ in Eq. (28). Then, we take advantage of the Baker-Campbell-Hausdorff formula, and omit terms $\sim \Delta t^2$ to formally integrate Eq. (28) term by term. The derivative operator (29) was handled by means of the Crank-Nicholson algorithm, and the Runge-Kutta algorithm was used in the last term of Eq. (28). We employed the spatial and temporal steps $\Delta x = \Delta y = 0.1$ and $\Delta t = 0.01$, respectively. The input was chosen as $\psi(x,y,0) = \pi^{-1/4}\exp\left(-x^2/2\right)$, and the output was picked up when the convergence of the energy attained the level of 10^{-8} (or after 10^4 iterations, in the case of unstable solutions).

The stability of the solutions obtained by the ITP method was checked by subsequent real-time simulations (RTS) of Eq. (8) for the evolution of perturbed stationary profiles, to which we have added random perturbations at the 5% amplitude level. A detailed discussion of these numerical methods is given in Ref. [56].

A. Repulsive interatomic interactions

Here, we consider the BEC with the repulsive nonlinearity ($g > 0$), trapped in HO potential

$$V(x,y) = \frac{\lambda^2}{2}(x^2 + y^2), \tag{31}$$

with $\lambda \equiv \omega_\perp/\omega_x \ll 1$ representing the anisotropy of the HO confinement.

First, we set $g = 1$, to address the low-density case, $g|f|^2 \ll 1$. In Fig. 2 we display the numerical results for

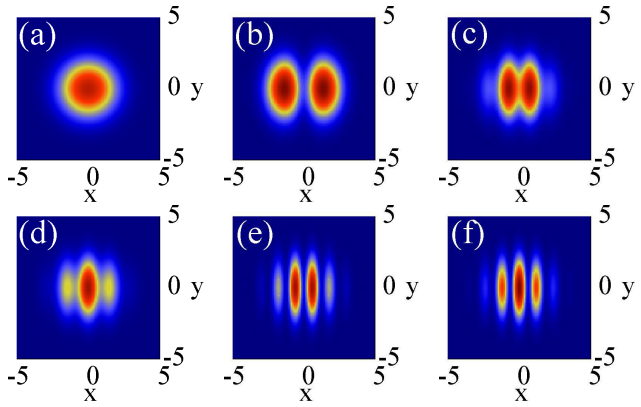

Figure 2: (Color online) Density profile $|f|^2$ produced by Eq. (12) for (a) $\gamma = 1$ and $\Gamma = 0$; (b) $\gamma = 1$ and $\Gamma = 1$; (c) $\gamma = 2$ and $\Gamma = 1$; (d) $\gamma = 2$ and $\Gamma = -1$; (e) $\gamma = 3$ and $\Gamma = 5$; (f) $\gamma = 3$ and $\Gamma = -5$; we use $g = 1$ ($\max\left[g|f|^2\right] \simeq 0.1$) and $\lambda = 1/3$ in all cases.

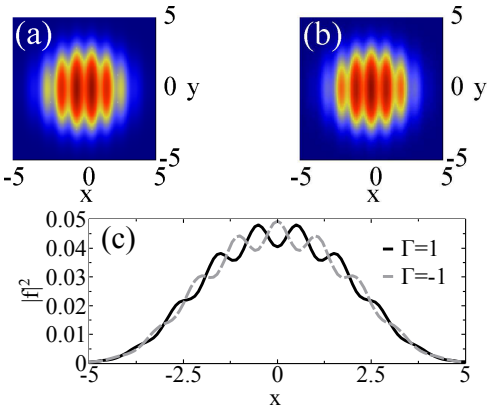

Figure 3: (Color online) Density profile $|f|^2$ produced by Eq. (12) for (a) $\Gamma = 1$ and (b) $\Gamma = -1$. (c) Cross-section profiles in x-direction, $|f(x,0)|^2$, corresponding to cases (a) (the solid black line) and (b) (the dashed gray line). (c) In both cases we have used $g = 20$ ($\max\left[g|f|^2\right] \simeq 1$), $\lambda = 1/3$, and $\gamma = 3$.

different values of the SO and Rabi constants, γ and Γ. As shown in Fig. 2(a), for $\Gamma = 0$ the ground state does not feature an oscillation pattern, while Fig. 2(b) displays the influence of positive Γ on the solution. Note that in Figs. 2(c) and 2(e), for $\Gamma < \gamma$ and $\Gamma > \gamma$, respectively, the results show the emergence of spatial oscillations in the solution, with an amplitude approximately proportional to Γ/γ^2 or γ/Γ, cf. Eqs. (22) and (18), respectively. We stress the importance of sign of Γ, which determines a peak or a hole at the center of the solution, as can be seen in Figs. 2(d) and 2(f), demonstrating the inverted sign with respect to that in Figs. 2(c) and 2(e), respectively. This result is also emphasized in the high-density limit, as shown in Fig. 3 for $\Gamma = 1$ and $\Gamma = -1$ [Figs. 3(a) and 3(b), respectively], setting $g = 20$, $\lambda = 1/3$, and $\gamma = 3$ in both cases. Also, in Fig. 3(c) we present, for the sake of comparison, two cross-section profiles drawn through $y = 0$.

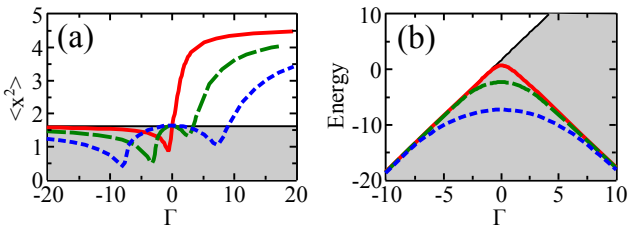

Figure 4: (Color online) (a) The squared width, $\langle x^2 \rangle$, and (b) the energy of the solitons versus the Rabi coupling, Γ. The boundary of the gray region corresponds to the respective value for $\gamma = 0$, while $\gamma = 1$ is represented by the red solid line, $\gamma = 2$ – by the green long-dashed-line, and $\gamma = 3$ – by the dashed-line blue line. The other parameters are $g = 1$ and $\lambda = 1/3$.

In Fig. 4(a) we display the average squared width,

$$\langle x^2 \rangle = \int_{-\infty}^{+\infty} \int_{-\infty}^{+\infty} x^2 |f|^2 dx dy, \tag{32}$$

versus Γ for different values of γ, with f obtained numerically from Eq. (12). Here, as well as in Fig. 2, the influence of the sign of Γ on the form of the solution is evident. At $\Gamma > 0$ the splitting in the solution profile is such that the squared width is larger than its value at $\gamma = 0$. The corresponding energies versus Γ are shown in Fig. 4(b).

B. Attractive interatomic interactions

In this subsection we deal with the attractive nonlinearity ($g < 0$), with the corresponding sign changes in Eq. (16). First, we aim to investigate effects of the SO and Rabi couplings on bright solitons by solving Eqs. (8) and (12) with $g < 0$, in the absence of the axial trapping potential [$V(x,y) = 0$], following the similar analysis reported in Ref. [39] for the usual cubic nonlinearity.

For $\gamma = 0$ and/or $\Gamma = 0$, with $V(x,y) = 0$ in Eqs. (8) and (12), all solutions are unstable, as should be expected for 2D free-space solitons in the case of the self-attraction. However, it was found in Ref. [39] that two-component BEC with the SO Rashba coupling and cubic attractive interactions gives rise to stable solitons of two types: semi-vortices (with a vortex in one component and a fundamental soliton in the other), or mixed modes (with topological charges 0 and ± 1 mixed in both components). Here, we report numerical observation of a stable composite bright solitons, following a scenario different from that shown in Ref. [39]: we consider the Rashba-equal-Dresselhaus coupling, while in Ref. [39] the Rashba-only SO term was analyzed. Note that, in the case of the attractive interactions ($g < 0$), our solution does not represent the ground state, which formally corresponds to the collapse in the 2D setting.

To highlight the possible stability regions for 2D solitons, we look first for solutions with a small width, measured as per definition (32). The squared width, $\langle x^2 \rangle$, and the energy for states supported by the attractive interaction are displayed in

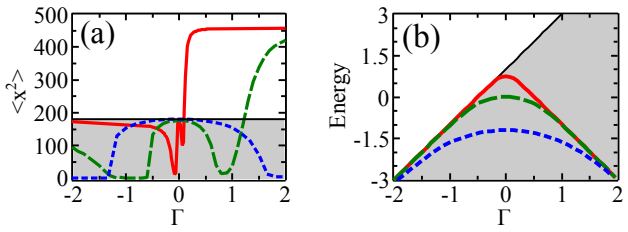

Figure 5: (Color online) (a) The squared width, $\langle x^2 \rangle$, and (b) the energy of the solitons versus the Rabi coupling Γ for BEC with the attractive interactions ($g = -3$). The boundary of the gray region corresponds to $\gamma = 0$, while $\gamma = 0.5$ corresponds to the red solid line, $\gamma = 1$ – to the green long-dashed-line, and $\gamma = 1.5$ – to the blue dashed line. We use $\lambda = 0$ (free space).

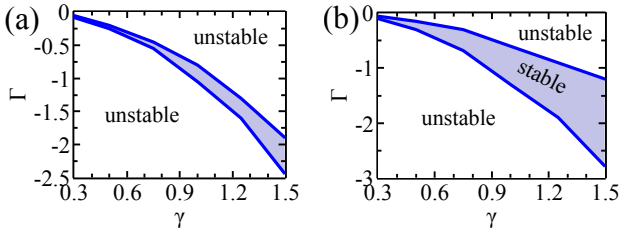

Figure 6: (Color online) Stability region for the ground-state soliton solutions, as a function of the SO and Rabi coupling strengths. We set $g = -1$ in (a) and $g = -3$ in (b), both with $\lambda = 0$ (free space). Stable solutions are found in the highlighted regions for $\Gamma < 0$.

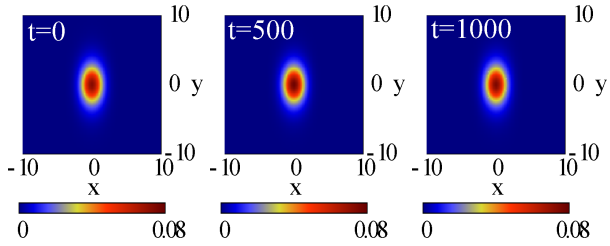

Figure 7: (Color online) The stable evolution in the free space ($\lambda = 0$) of the perturbed solution, $|F_1|^2$, whose stationary form was produced by the ITP method for $g = -3$, $\gamma = 1$, and $\Gamma = -1$ [note that this point belongs to the stability region in Fig. 6(b)]. A similar result (not shown here) is obtained for the other component, $|F_2|^2$.

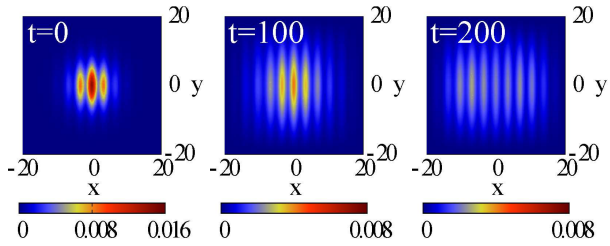

Figure 8: (Color online) The unstable evolution in the free space ($\lambda = 0$) of the perturbed solution, $|F_1|^2$, whose stationary form was produced by the ITP method for $g = -3$, $\gamma = 1$, and $\Gamma = -0.4$ [note that this point belongs to the instability region in 6(b)]. A similar result (not shown here) is obtained for the other component, $|F_2|^2$.

Fig. 5(a) and 5(b), respectively, as a function of Γ for $\gamma = 0.5$ by the red solid line, for $\gamma = 1$ by the green long-dashed-line, and for $\gamma = 1.5$ by the blue dashed line. The boundary of the gray region shows the values in the absence of the SO coupling ($\gamma = 0$). Note that the squared width is more sensitive to the variation of Γ in comparison to the case of the repulsive interaction, cf. Fig. 4(a). However, the energy of the solutions shows a pattern similar to that observed in the repulsive system, cf. Fig. 4(b). Actually, minima of the squared width are linked to the stability regions, see below.

In Fig. 6 we show the main result of this subsection, *viz.*, *stability regions* for the 2D free-space solitons for (a) $g = -1$ and (b) $g = -3$, as produced by direct RTS of the perturbed evolution of stationary solutions that were obtained by means of the ITP method. For $\Gamma < 0$ we find a region of stable single-peak solutions, while for $\Gamma > 0$ all the solutions are unstable (at least, for $\Gamma < 2$). Note that the stability region slightly increases with the increase of the strength of the nonlinearity.

As might be expected, the stability of the solutions obtained by the ITP method has been corroborated by subsequent real-time simulations (RTS) of Eq. (8). In Figs. 7 and 8, respectively, we show examples of the stable and unstable real-time evolution of perturbed stationary solutions that were supplied by the ITP method. All stable solutions that we have found are fundamental solitons (in contrast to stable semi-vortices and mixed modes obtained in Ref. [39]), with a single-peak shape similar to that observed in Fig. 7.

Next, we consider the same system, but in presence of the HO potential, taken as in Eq. (31). Our goal is to extend the stability, with the help of the confining potential, to $\Gamma > 0$, when all the free-space solitons are unstable. In Fig. 9 we present the numerical results obtained for different values of the SO (γ) and Rabi (Γ) couplings. For a fixed value of Γ [e.g., $\Gamma = -1$ in Figs. 9(a-c) and $\Gamma = 1$ in Figs. 9(d-f)] and increasing γ, we observe an increase of the number of spatial oscillations of the solution, and, consequently, a reduction in its amplitude, as predicted by approximated solution (22). Eventually, as well as in the case of the repulsive interatomic interactions, we have numerically verified that the HO trapping potential stabilizes the ground-state solutions displayed in Fig. 9.

IV. CONCLUSION

Starting from the full 3D system of the GP equations for the binary BEC, including the SO (with equal Rashba and Dresselhaus terms) and Rabi couplings, we have derived a system of two coupled 2D NPSEs (nonpolynomial Schrödinger equations) for the SO-coupled BEC in the pancake-shaped configuration. Further, assuming that the strengths of the nonlinear interactions between different atomic states are equal, we have reduced the stationary version of the system to the single nonlinear equation, for a given chemical potential. This simplification has allowed us to obtain simple approximate analyt-

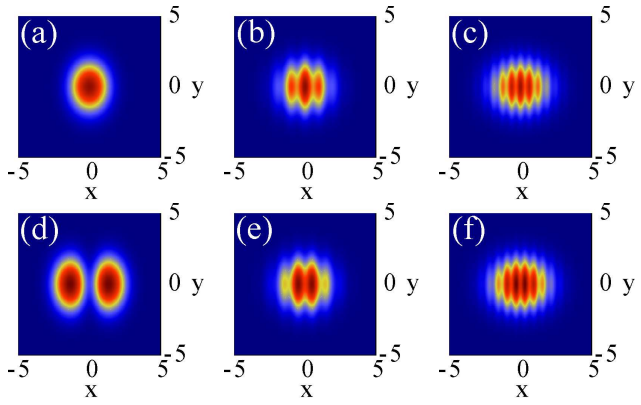

Figure 9: (Color online) Density profile $|f|^2$ obtained from the numerical solution of Eq. (12), which includes the trapping potential (31), for (a) $\Gamma = -1$ and $\gamma = 1$; (b) $\Gamma = -1$ and $\gamma = 3$; (c) $\Gamma = -1$ and $\gamma = 5$; (d) $\Gamma = 1$ and $\gamma = 1$; (e) $\Gamma = 1$ and $\gamma = 3$; (f) $\Gamma = 1$ and $\gamma = 5$. Here, we set $g = -1$ and $\lambda = 1/3$ in all the cases.

ical solutions, and consider the low- and high-density limits. By means of systematic simulations, we have obtained localized solutions in perfect agreement with the analytical predictions. In the case of the attractive interactions, the most essential result is finding the *stability area* for the 2D fundamental (single-peak) solitons in the *free space*, which is impossible without the SO and Rabi couplings.

The analysis can be naturally extended by incorporating more general forms of the SO coupling, as well as by including spatially inhomogeneous nonlinearity, which may induce an effective nonlinear potential for solitons.

Acknowledgments

L.S. appreciates partial support from Universitá di Padova (Research Project “Quantum Information with Ultracold Atoms in Optical Lattices"), Cariparo Foundation (Excellence Project “Macroscopic Quantum Properties of Ultracold Atoms under Optical Confinement"), and Ministero Istruzione Universita Ricerca of Italy (PRIN Project “Collective Quantum Phenomena: from Strongly-Correlated Systems to Quantum Simulators"). W.B.C. thanks Brazilian agencies CNPq and the National Institute of Science and Technology for Quantum Information (INCT-IQ) for partial support. The work of B.A.M. was supported, in a part, by the German-Israel Foundation through grant No. I-1024-2.7/2009, and by the Binational Science Foundation (US-Israel) through grant No. 2010239.

[1] M. H. Anderson, J. R. Ensher, M. R. Matthews, C. E. Wieman, and E. A. Cornell, Science **269**, 198 (1995).
[2] K. B. Davis, M.-O. Mewes, M. R. Andrews, N. J. van Druten, D. S. Durfee, D. M. Kurn, and W. Ketterle, Phys. Rev. Lett. **75**, 3969 (1995).
[3] C. C. Bradley, C. A. Sackett, J. J. Tollett, and R. G. Hulet, Phys. Rev. Lett. **75**, 1687 (1995).
[4] F. Dalfovo, S. Giorgini, L. P. Pitaevskii, and S. Stringari, Rev. Mod. Phys. **71**, 463 (1999).
[5] J. Billy, V. Josse, Z. Zuo, A. Bernard, B. Hambrecht, P. Lugan, D. Clément, L. Sanchez-Palencia, P. Bouyer, and A. Aspect, Nature **453**, 891 (2008).
[6] G. Roati, C. D’Errico, L. Fallani, M. Fattori, C. Fort, M. Zaccanti, G. Modugno, M. Modugno, and M. Inguscio, Nature **453**, 895 (2008).
[7] L. Khaykovich, F. Schreck, G. Ferrari, T. Bourdel, J. Cubizolles, L. D. Carr, Y. Castin, and C. Salomon, Science **296**, 1290 (2002).
[8] K. E. Strecker, G. B. Partridge, A. G. Truscott, and R. G. Hulet, Nature (London) **417**, 150 (2002).
[9] S. L. Cornish, S. T. Thompson, and C. E. Wieman, Phys. Rev. Lett. **96**, 170401 (2006).
[10] A. L. Marchant, T. P. Billam, T. P. Wiles, M. M. H. Yu, S. A. Gardiner, and S. L. Cornish, Nature Commun. **4**, 1865 (2013).
[11] S. Burger, K. Bongs, S. Dettmer, W. Ertmer, K. Sengstock, A. Sanpera, G. V. Shlyapnikov, and M. Lewenstein, Phys. Rev. Lett. **83**, 5198 (1999).
[12] C. Becker, S. Stellmer, P. Soltan-Panahi, S. Dörscher, M. Baumert, E.-M. Richter, J.Kronjäger, K. Bongs, and K. Sengstock, Nature Phys. **4**, 496 (2008).
[13] M. R. Matthews, B. P. Anderson, P. C. Haljan, D. S. Hall, C. E. Wieman, and E. A. Cornell , Phys. Rev. Lett. **83**, 2498 (1999).
[14] T. W. Neely, E. C. Samson, A. S. Bradley, M. J. Davis, and B. P. Anderson, Phys. Rev. Lett. **104**, 160401 (2010).
[15] D. V. Freilich, D. M. Bianchi, A. M. Kaufman, T. K. Langin, and D. S. Hall, Science **329**, 1182 (2010).
[16] J. A. Seman, E. A. L. Henn, M. Haque, R. F. Shiozaki, E. R. F. Ramos, M. Caracanhas, P. Castilho, C. Castelo Branco, P. E. S. Tavares, F. J. Poveda-Cuevas, G. Roati, K. M. F. Magalhães, and V. S. Bagnato, Phys. Rev. A **82**, 033616 (2010).
[17] S. Middelkamp, P. J. Torres, P. G. Kevrekidis, D. J. Frantzeskakis, R. Carretero-González, P. Schmelcher, D. V. Freilich, and D. S. Hall, Phys. Rev. A **84**, 011605(R) (2011).
[18] C. Ryu, M. F. Andersen,P. Clade, V. Natarajan, K. Helmerson, and W. D. Phillips, Phys. Rev. Lett. **99**, 260401 (2007).
[19] A. Ramanathan, K. C. Wright, S. R. Muniz, M. Zelan, W. T. Hill, C. J. Lobb, K. Helmerson, W. D. Phillips, and G. K. Campbell, Phys. Rev. Lett. **106**, 130401 (2011).
[20] S. Wuester, T. E. Argue, and C. M. Savage, Phys. Rev. A **72**, 043616 (2005).
[21] Y.-J. Lin, R. L. Compton, K. Jiménez-García,W. D. Phillips, J. V. Porto and I. B. Spielman, Nature Phys. **7**, 531 (2011).
[22] Y.-J. Lin, K. Jiménez-García, and I. B. Spielman, Nature **471**, 83 (2011).
[23] T. Kinoshita, T. Wenger and D. S. Weiss, Nature **440**, 900 (2006).
[24] T. L. Ho and S. Z. Zhang, Phys. Rev. Lett. **107**, 150403 (2011).
[25] X.-Q. Xu and J. H. Han, Phys. Rev. Lett. **107**, 200401 (2011).
[26] J. Radic, T. A. Sedrakyan, I. B. Spielman, and V. Galitski, Phys. Rev. A **84**, 063604 (2011).
[27] X. F. Zhou, J. Zhou, and C. J. Wu, Phys. Rev. A **84**, 063624 (2011).
[28] S. Sinha, R. Nath, and L. Santos, Phys. Rev. Lett. **107**, 270401 (2011).

[29] H. Hu, B. Ramachandhran, H. Pu, and X.-J. Liu, Phys. Rev. Lett. **108**, 010402 (2012).

[30] B. Ramachandhran, B. Opanchuk, X.-J. Liu, H. Pu, P. D. Drummond, and H. Hu, Phys. Rev. A **85**, 023606 (2012).

[31] R. Barnett, S. Powell, T. Graβ, M. Lewenstein, and S. Das Sarma, Phys. Rev. A **85**, 023615 (2012).

[32] Y. Deng, J. Cheng, H. Jing, C.-P. Sun, and S. Yi, Phys. Rev. Lett. **108**, 125301 (2012).

[33] L. Wen, Q. Sun, H. Q. Wang, A. C. Ji, and W. M. Liu, Phys. Rev. A **86**, 043602 (2012).

[34] D. A. Zezyulin, R. Driben, V. V. Konotop, and B. A. Malomed, Phys. Rev. A **88**, 013607 (2013).

[35] Y. Xu, Y. Zhang, and B. Wu, Phys. Rev. A **87**, 013614 (2013).

[36] V. Achilleos, D. J. Frantzeskakis, P. G. Kevrekidis, and D. E. Pelinovsky, Phys. Rev. Lett. **110**, 264101 (2013).

[37] Y. V. Kartashov, V. V. Konotop, and F. Kh. Abdullaev, Phys. Rev. Lett. **111**, 060402 (2013).

[38] L. Salasnich and Boris A. Malomed, Phys. Rev. A **87**, 063625 (2013).

[39] H. Sakaguchi, B. Li, and B. A. Malomed, Phys. Rev. E **89**, 032920 (2014).

[40] V. E. Lobanov, Y. V. Kartashov, and V. V. Konotop, Phys. Rev. Lett. **112**, 180403 (2014).

[41] V. Achilleos, J. Stockhofe, P. G. Kevrekidis, D. J. Frantzeskakis, and P. Schmelcher, EPL **103**, 20002 (2013).

[42] L. Berge, Phys. Rep. **303**, 259 (1998); E. A. Kuznetsov and F. Dias, *ibid*. **507**, 43 (2011).

[43] P.-S. He, Eur. Phys. J. D **67**, 48 (2013).

[44] P.-S. He, W.-L. You, and W.-M. Liu, Phys. Rev. A **87**, 063603 (2013).

[45] H. Sakaguchi and B. Li, Phys. Rev. A **87**, 015602 (2013).

[46] A. L. Fetter, Phys. Rev. A **89**, 023629 (2014).

[47] B. Li and H. Sakaguchi, J. Low Temp. Phys. **175**, 243 (2014).

[48] Y. S. Cheng, G. H. Tang, and S. K. Adhikari, Phys. Rev. A **89**, 063602 (2014).

[49] J. Jin, S. Zhang, and W. Han, J. Phys. B: At. Mol. Opt. Phys. **47**, 115302 (2014).

[50] S.-W. Song, Y.-C. Zhang, H. Zhao, X. Wang, and W.-M. Liu, Phys. Rev. A **89**, 063613 (2014).

[51] L. Zhou, H. Pu, and W. Zhang, Phys. Rev. A **87**, 023625 (2013).

[52] L. Salasnich, Laser Phys. **12**, 198 (2002); L. Salasnich, A. Parola, and L. Reatto, Phys. Rev. A **65**, 043614 (2002).

[53] A. Muñoz Mateo and V. Delgado, Phys. Rev. A **77**, 013617 (2008); Ann. Phys. (N.Y.) **324**, 709 (2009).

[54] L. P. Pitaevskii and A. Stringari, *Bose-Einstein Condensation* (Clarendon Press: Oxford, 2003).

[55] L. Salasnich and B. A. Malomed, Phys. Rev. A **79**, 053620 (2009).

[56] P. Muruganandam and S. K. Adhikari, Comput. Phys. Commun. **180**, 1888 (2009), and references therein.